Industrial Engineering
2026, Vol. 15, No. 3, pp. 53–63
https://doi.org/10.11648/j.ijiis.20261503.11

Research Article

Modelling and Simulation of Engineering Design, A Second-Order Differential Equations in Mechanical and Electrical Systems

George Chikwendu Ihenacho[1], Diarah Reuben Samuel[2, *], Osueke Christian Okechukwu[2], Samuel Adebanji Ajayi[2], Evoh Edwin Emeng[3], Oluwasade Kehinde[2], Olaomi Bimpe Agnes[4]

[1]Mechanical Engineering Department, Pan-Atlantic University, Lekki, Nigeria
[2]Mechatronics Engineering Program, Bowen University, Iwo, Nigeria
[3]Mechatronics Engineering Department, Federal University, Oye Ekiti, Nigeria
[4]Ladoke Akintola Universityof Technology, Ogbomoso, Nigeria

Abstract

This paper presents a rigorous and systematic investigation into the fundamental role of second-order ordinary differential equations (ODEs) in the modelling, analysis, and design of engineering systems. The study is anchored on two canonical and cross-disciplinary case studies: the quarter-car suspension system and the series RLC circuit. For each system, the governing differential equations are derived from first principles using Newtonian and Kirchhoffian formulations, respectively, followed by complete analytical solutions obtained via the characteristic (auxiliary) equation framework.The classical dynamic response includes underdamped, critically damped, and overdamped are comprehensively analyzed, with explicit linkage to practical engineering design criteria. In particular, damping ratio targets are contextualized within industry standards, where passenger vehicle suspensions typically operate within $\zeta \approx 0.3$–0.4 to ensure ride comfort, while high-performance systems adopt $\zeta \approx 0.65$–0.70 to achieve improved transient response characteristics. The forced harmonic response is further examined, with emphasis on resonance behavior, amplitude amplification, and stability considerations, highlighting its critical implications for structural integrity and failure prevention, as exemplified by the Tacoma Narrows Bridge collapse. A unified cross-domain analytical framework is established, demonstrating that mechanically and electrically distinct systems are governed by mathematically analogous second-order ODEs. This analogy enables the transfer of insights and design strategies across engineering domains. Furthermore, numerical solutions obtained using the Euler method and the fourth-order Runge–Kutta (RK4) algorithm are systematically benchmarked against exact analytical solutions. Convergence and error analyses confirm the superior accuracy of RK4 with global truncation error of order $O(h^4)$, compared to the first-order accuracy $O(h)$ of the Euler method. The paper concludes by highlighting key design implications and emphasizing the transformative role of simulation-driven engineering in accelerating system development, optimizing performance, and reducing reliance on costly experimental prototyping.

*Correspondence: Diarah Reuben Samuel (diarah.samuel@bowen.edu.ng)

Received: 4 April 2026; **Accepted:** 20 April 2026; **Published:** 22 September 2026

Keywords

Second-order ODE, Mass-spring-damper, RLC Circuit, Damping Ratio, Natural Frequency, Resonance, Numerical Simulation, Runge-Kutta, Engineering Design

1. Introduction

The ability to predict the dynamic behaviour of an engineering system before committing to physical construction is one of the most economically valuable capabilities in modern engineering practice. At the heart of this predictive power lies mathematical modelling the translation of physical laws into equations that faithfully capture how a system evolves over time. Among the many mathematical tools available, ordinary differential equations (ODEs) occupy a privileged position because they describe the time evolution of virtually any lumped-parameter system, from the bounce of a car suspension to the ringing of a telephone circuit [1, 2].

Second-order ODEs are of particular engineering importance because they arise naturally whenever a system stores energy in two distinct modes simultaneously. In a mechanical oscillator, energy alternates between kinetic (stored in a moving mass) and potential (stored in a compressed or extended spring); in an RLC circuit, energy alternates between a magnetic field (inductor) and an electric field (capacitor). This dual-storage character is what gives second-order systems their rich dynamic repertoire: oscillation, resonance, transient decay, and steady-state response [3, 4].

Simulation converts an abstract differential equation into a concrete, time-resolved trajectory that a designer can inspect, manipulate, and optimize. The rise of numerical computing tools which includes MATLAB/Simulink, Python's SciPy/NumPy ecosystem, and domain-specific modelling languages such as Modelica has transformed simulation from a specialist activity into a routine step in engineering design. Modern automotive OEMs, for example, routinely build and analyse hundreds of virtual suspension configurations before building a single physical prototype [5, 6].

This paper develops the theme of simulation-based design around a focused case-study approach. Section 2 establishes the mathematical foundation. Sections 3 and 4 present the mechanical and electrical case studies respectively, including derived equations, analytical solutions, and simulation results. Section 5 addresses the forced response and the resonance phenomenon. Section 6 formalizes the cross-domain analogy. Section 7 compares numerical methods. Section 8 synthesizes the design implications, and Section 9 concludes.

2. Mathematical Foundation of Second-Order ODEs

2.1. General Form and Classification

A linear, constant-coefficient second-order ODE takes the standard form:

$$a \cdot y''(t) + b \cdot y'(t) + c \cdot y(t) = f(t) \tag{1}$$

where $y(t)$ is the dependent variable of physical interest (displacement, charge, angle, etc.), the prime notation denotes differentiation with respect to time t, constants $a, b, c > 0$ are determined by system parameters, and $f(t)$ is the external forcing function. When $f(t) \equiv 0$ the equation is called homogeneous (representing free, undriven response); when $f(t) \neq 0$ it is non-homogeneous (forced response). The general solution to the non-homogeneous case is the sum of the complementary function (homogeneous solution) and a particular integral [7].

2.2. The Characteristic Equation and Its Roots

The homogeneous solution is found by substituting the trial solution y(t) = e^(st) into equation (1) and dividing by e^(st), yielding the characteristic (auxiliary) equation:

$$a \cdot s^2 + b \cdot s + c = 0 \tag{2}$$

The discriminant $\Delta = b^2 - 4ac$ partitions the solution space into three qualitatively distinct regimes whose physical significance is profound:

$\Delta < 0 \rightarrow$ complex conjugate roots $\rightarrow$ oscillatory decay (underdamped)

$\Delta = 0 \rightarrow$ repeated real root $\rightarrow$ fastest settling (critically damped)

$\Delta > 0 \rightarrow$ two distinct real roots $\rightarrow$ sluggish return (overdamped)

2.3. Canonical Parameters: ω_n and ζ

Dividing equation (1) through by a and introducing two physically interpretable parameters the undamped natural frequency ω_n and the dimensionless damping ratio ζ casts the ODE in its most useful engineering form:

$$y'' + 2\zeta\omega_n \cdot y' + \omega_n^2 \cdot y = f(t)/a \tag{3}$$

where y(t) is the system response, and f(t) is the external forcing function. The system parameters are defined as follows:

$$\omega_n = \sqrt{c/a} \text{ [rad/s]}$$

$$\zeta = b / (2\sqrt{ac}) \text{ [dimensionless]}$$

The parameter ω_n represents the frequency at which the system would oscillate if there were no damping whatsoever. The damping ratio ζ is the single most important design parameter for a second-order system: it determines whether the system oscillates, how quickly it settles to steady state, and whether it overshoots a target value. A damping ratio of zero gives perpetual oscillation; a ratio of one gives the critically damped (fastest non-oscillatory) response; ratios greater than one give sluggish overdamped responses. The three solution forms are summarised in Table 2 (Section 5) [3, 7].

3. Case Study I — Quarter-Car Suspension System

3.1. Physical Model and Motivation

The suspension system of a road vehicle is one of the most consequential engineering applications of second-order ODE modelling. Its primary function is to isolate the vehicle body (sprung mass) from road disturbances while maintaining tyre contact with the road surface, thereby balancing ride comfort against handling responsiveness, two requirements that are fundamentally in tension [5, 8].

The quarter-car model reduces one corner of the vehicle to a single-degree-of-freedom (SDOF) mass-spring-damper system. A rigid sprung mass m (kg) representing the vehicle body is connected through a coil spring of stiffness k (N/m) and a viscous shock absorber (dashpot) with damping coefficient c (N·s/m) to a fixed road surface. Road inputs are modelled as an initial displacement or as a prescribed time-varying profile.

3.2. Equation of Motion

Applying Newton's second law (ΣF = ma) to the sprung mass in the vertical direction, with the spring force opposing displacement and the dashpot force opposing velocity:

$$m \cdot x''(t) + c \cdot x'(t) + k \cdot x(t) = F(t) \quad (4)$$

where x(t) is vertical displacement from the static equilibrium position and F(t) is any external road or load disturbance. This is precisely equation (1) with a = m, b = c, c = k. The defining parameters are:

$$\omega_n = \sqrt{k/m} \text{ [rad/s]} \quad \zeta = c / (2\sqrt{mk}) \text{ [dimensionless]}$$

$$\omega d = \omega_n\sqrt{1 - \zeta^2} \text{ [rad/s, damped natural frequency, valid for } \zeta < 1]$$

3.3. Free Response — Three Damping Regimes

Underdamped response (ζ < 1)

When ζ < 1, the characteristic roots are complex conjugates $s_{1,2} = -\zeta\omega_n \pm j\omega d$. The solution oscillates at frequency ωd with exponentially decaying amplitude:

$$x(t) = A \cdot e\text{^}(-\zeta\omega_n t) \cdot \sin(\omega d \cdot t + \varphi) \quad (5)$$

where A and φ are determined by initial conditions. The system crosses equilibrium repeatedly, a behaviour that in a vehicle suspension manifests as bouncing after a bump — uncomfortable for passengers and potentially dangerous for tyre contact [5].

Critically damped response (ζ = 1)

When ζ = 1, the characteristic equation yields a repeated real root $s = -\omega_n$. The solution is:

$$x(t) = (C_1 + C_2 t) \cdot e\text{^}(-\omega_n t) \quad (6)$$

This returns to equilibrium in the shortest possible time without oscillation. It is therefore the theoretical ideal for a vehicle suspension no bouncing, fastest response. In practice, however, exact critical damping is impossible to achieve because any small uncertainty in mass (varying passenger loads) or temperature-dependent shock absorber viscosity shifts the system into the underdamped or overdamped regime [5, 8].

Overdamped response (ζ > 1)

When ζ > 1, the characteristic roots are two distinct negative real numbers s_1, s_2. The solution is a sum of two decaying exponentials:

$$x(t) = A_1 \cdot e\text{^}(s_1 t) + A_2 \cdot e\text{^}(s_2 t) \quad (7)$$

The response is slow and sluggish a very stiff, over-damped suspension transmits more road force into the vehicle body, degrading ride comfort significantly. It is appropriate only in specific applications (e.g., large freight vehicles prioritising stability over comfort, or NASCAR aerodynamic dampers requiring very low ride height) [9, 10].

3.4. Simulation Results — Suspension Design

Figure 1 presents simulation results for a representative quarter-car model with sprung mass m = 300 kg and spring stiffness k = 24,000 N/m (giving $\omega_n \approx 8.9$ rad/s, approximately 1.4 Hz a typical passenger car body frequency). An initial displacement of 60 mm simulates a sharp road bump. Four damping configurations are compared.

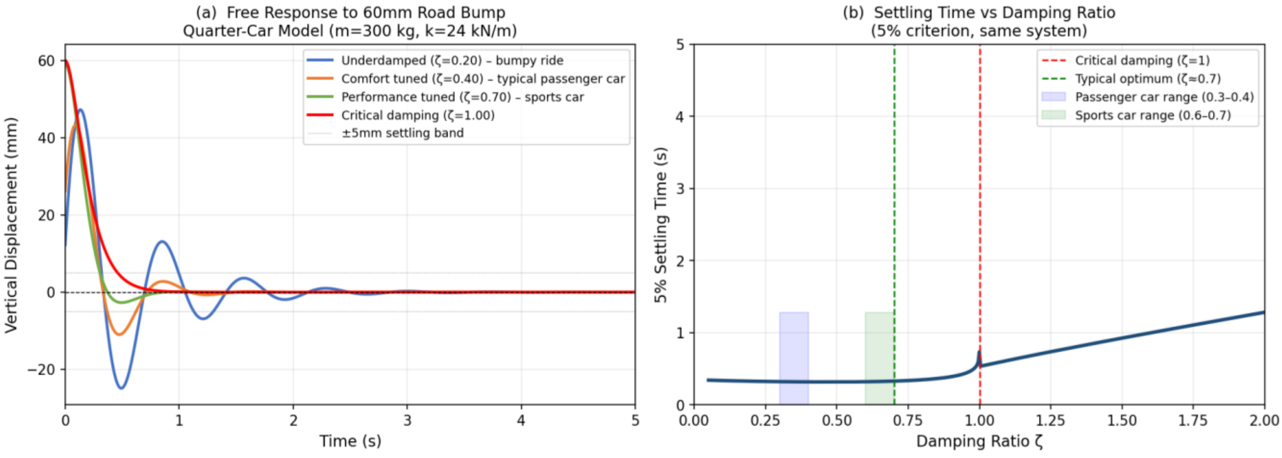

Figure 1. *Quarter-Car Suspension System. (a) Free response to a 60 mm road bump for four damping configurations. Comfort-tuned vehicles (ζ = 0.3–0.4) accept some oscillation in exchange for a softer ride; performance vehicles (ζ = 0.65–0.70) settle faster but with a harder ride. (b) 5% settling time as a function of ζ, demonstrating that $\zeta \approx 0.7$ minimises settling time while remaining robustly non-critical.*

Panel (a) reveals the fundamental ride-comfort vs. handling trade-off: lower ζ produces multiple oscillations after the bump (acceptable in a luxury saloon but unacceptable in a sports car), while higher ζ returns the body quickly to equilibrium. Panel (b) identifies the settling-time minimum at $\zeta \approx 0.7$ a result consistent with published suspension design guidelines. Samant et al. [10] confirmed through quarter-car modelling that a damping ratio of $\zeta = 0.7$ represents the optimum across ride comfort, wheel displacement, and handling metrics. FIRGELLI Automations [8] notes that targeting $\zeta \approx 0.7$ provides 5% overshoot and fast settling while remaining robust to ±10% parameter uncertainty — achieving exactly critical damping is impractical since a 10% error shifts ζ from 1.0 to 0.91 or 1.10, both of which restore oscillatory or sluggish behaviour respectively.

4. Case Study II — Series RLC Circuit

4.1. Physical Description

The series RLC circuit is the electrical archetype of a second-order system. It consists of a resistor R (Ω), an inductor L (H), and a capacitor C (F) connected in series with a voltage source E(t). The circuit contains two energy-storage elements the inductor's magnetic field and the capacitor's electric field whose interaction produces oscillatory behaviour entirely analogous to the mass-spring-damper. RLC circuits are described as second-order circuits precisely because two energy-storage elements produce a governing second-order differential equation [11, 12].

Practical RLC applications include: radio and television tuner circuits (band-pass filters exploiting resonance to select narrow frequency bands); power-factor correction circuits in industrial supplies; switched-mode power supply resonant converters; and oscillator circuits for signal generation. Understanding the damping regime is therefore directly connected to filter bandwidth, signal integrity, and power efficiency [11].

4.2. Governing Equation

Applying Kirchhoff's Voltage Law around the series loop and using the constitutive relations VL = L(di/dt), VR = Ri, VC = q/C, with i = dq/dt:

$$L \cdot q''(t) + R \cdot q'(t) + (1/C) \cdot q(t) = E(t) \quad (8)$$

This is exactly equation (1) with a = L, b = R, c = 1/C. The natural frequency and damping parameters are:

$$\omega_0 = 1/\sqrt{LC} \text{ [rad/s]}$$

$$\alpha = R/(2L) \text{ [Np/s, attenuation factor]}$$

$$\zeta = (R/2) \cdot \sqrt{C/L} \text{ [dimensionless]}$$

The condition for critical damping is $R = 2\sqrt{L/C}$ — halving the resistance makes the circuit underdamped and introduces ringing; doubling it makes the circuit overdamped and sluggish.

4.3. Engineering Significance of the Three Regimes

In filter and oscillator design, the choice of damping regime determines the circuit's frequency selectivity. The Q-factor (quality factor), defined as $Q = \omega_0 L/R = 1/(2\zeta)$, captures this directly: high Q (low ζ, underdamped) produces sharp frequency selectivity desirable in radio tuners that must distinguish adjacent stations separated by only tens of kilohertz. Conversely, low Q (high ζ) produces a wide frequency bandwidth useful in broadband amplifiers. The bandwidth of the resonant peak is given by $BW = R/L = 2\alpha_n$ [11, 12].

Critical damping is sought in transient-pulse circuits where ringing would corrupt a digital signal edge for instance, termination resistors in high-speed printed circuit boards are chosen to achieve $\zeta \approx 1$ and suppress signal reflections. Overdamping is deliberately introduced in some measurement amplifiers to prevent the output from oscillating past the true value.

4.4. Simulation Results — RLC Natural Response

Figure 2 presents numerically computed natural current and capacitor voltage responses for L = 0.5 H, C = 20 mF (ω_0 = 10 rad/s), and V_0 = 12 V initial capacitor voltage. Critical damping occurs at $R = 2\sqrt{(L/C)} = 10\ \Omega$.

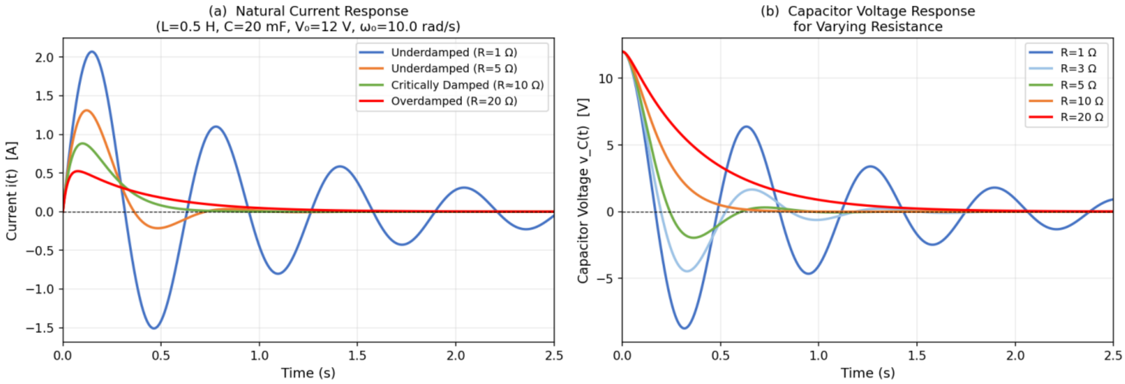

Figure 2. Series RLC Circuit Natural Response. (a) Current i(t) for four resistance values spanning all three damping regimes. (b) Capacitor voltage vC(t) for the same configurations, showing the familiar family of second-order responses. Parameters: L = 0.5 H, C = 20 mF (ω_0 = 10 rad/s), V_0 = 12 V.

The qualitative topology of Figure 2 mirrors Figure 1 precisely confirm the structural mathematical analogy between the two physically distinct systems. The critically damped circuit (R = 10 Ω) discharges smoothest and fastest, the underdamped cases ring, and the overdamped case (R = 20 Ω) discharges slowly. This is the engineer's key insight: understanding one system fully gives near-complete intuition about the other.

5. Forced Harmonic Response and the Resonance Phenomenon

5.1. Steady-State Solution Under Harmonic Excitation

When the forcing function takes the form $f(t) = F_0\cos(\omega t)$, the steady-state particular solution of equation (3) is also harmonic at frequency ω. After substitution and algebraic manipulation, the amplitude magnification factor H(ω) the ratio of output amplitude to the static deflection $F_0/(m\omega_n^2)$ is:

$$|H(\omega)| = 1 / \sqrt{[(1 - r^2)^2 + (2\zeta r)^2]} \tag{9}$$

where $r = \omega/\omega_n$ is the frequency ratio. This function is the Frequency Response Function (FRF) of the system. It shows how the system amplifies or attenuates excitation at different frequencies. For lightly damped systems ($\zeta \ll 1$), the peak amplification near r = 1 can be enormous the quality factor $Q = 1/(2\zeta)$ directly gives the peak amplitude magnification [3, 13].

5.2. Resonance and Design Implications

Figure 3(a) reveals several critical design insights. First, the peak amplification grows dramatically as ζ decreases — a structure with ζ = 0.05 experiences ten times more vibration at resonance than the static deflection would suggest. Second, the resonance peak shifts slightly below ω_n for damped systems (the precise peak occurs at $\omega r = \omega_n\sqrt{(1 - 2\zeta^2)}$). Third, well-damped systems (ζ > 0.7) show no distinct resonance peak at all their frequency response is essentially flat, a desirable property in broadband filters.

Figure 3(b) demonstrates the time-domain consequence: at resonance, energy is continuously fed into the system and the amplitude grows without bound (in the undamped limit) or to a large finite value (in the damped case). Off resonance, the transient homogeneous solution and the steady-state particular solution interfere to produce the 'beating' pattern visible in the blue trace, which settles quickly as the transient decays.

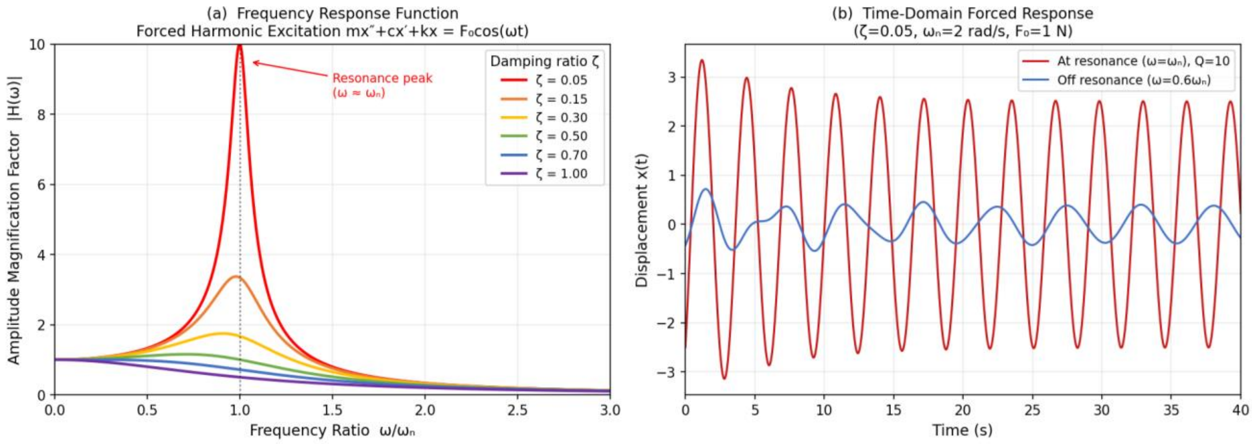

Figure 3. *Forced Harmonic Response. (a) Frequency response functions for six damping ratios, showing the resonance peak at* $r = \omega/\omega_n \approx 1$*. For* $\zeta = 0.05$*, the peak amplification reaches* $Q = 10$*; for* $\zeta = 0.01$ *it reaches* $Q = 50$ *— potentially catastrophic in structural applications. (b) Time-domain response of a lightly damped system (*$\zeta = 0.05$*) at resonance (red) vs. off-resonance (blue), demonstrating the progressive amplitude growth at resonance.*

5.3. Historical Case Study: The Tacoma Narrows Bridge (1940)

The 1940 collapse of the Tacoma Narrows Bridge in Washington State is the most cited structural failure in the engineering literature on second-order dynamics and also one of the most misunderstood. The original bridge, with a main span of 853 m, collapsed on 7 November 1940 under 64 km/h winds after experiencing growing torsional oscillations. The deck twisted in opposite directions at each end until the structure tore itself apart [14, 15].

Many undergraduate physics textbooks attributed the collapse to simple forced mechanical resonance the wind exciting the bridge at its torsional natural frequency but Billah and Scanlan [15] demonstrated conclusively that this interpretation is incorrect. Simple resonance requires the external forcing frequency to match the natural frequency precisely and stably, which turbulent wind cannot do. The actual mechanism was aeroelastic flutter: a self-excited oscillation in which the bridge's own motion generated aerodynamic forces at exactly the frequency needed to sustain and amplify the torsional mode. Mathematically, flutter corresponds to the effective damping coefficient b in the governing ODE becoming negative, making the characteristic root move into the right-half complex plane and producing exponentially growing oscillation [14].

The bridge's governing torsional ODE, in the Scanlan-Tomko model, takes the second-order form:

$$I \cdot \alpha'' + 2I\zeta\alpha\omega\alpha \cdot \alpha' + I\omega\alpha^2 \cdot \alpha = Q\_aero(\alpha, \alpha', U) \quad (10)$$

where I is the rotational inertia, ζα and ωα are the damping ratio and natural frequency of the torsional mode, and Q_aero captures the nonlinear aerodynamic coupling through bridge velocity U. At a critical wind speed, the aerodynamic term effectively cancelled and then reversed the positive structural damping, making the effective ζ negative and triggering the instability [14-16].

The engineering lesson is unambiguous: the simulation of dynamic response, including careful identification of natural frequencies and damping ratios under realistic loading conditions, is not merely academic. The bridge's fundamental flexibility (inadequate stiffening depth relative to span) gave it natural frequencies that, under aeroelastic coupling, became catastrophically unstable. Modern suspension bridge design mandates comprehensive aeroelastic wind-tunnel testing and dynamic simulation validated against the second-order ODE framework developed in this paper [14].

5.4. Cross-Domain Analogy and Parameter Mapping

The structural similarity between the mass-spring-damper and RLC circuit equations (4) and (8) is not coincidental. Both arise from the same physical principle energy conservation applied to a system with two storage modes and one dissipation mechanism. Table 1 formalises the complete parameter-by-parameter analogy.

Table 1. *Mechanical–Electrical Parameter Analogy for Second-Order Systems.*

Parameter	Mechanical System	Electrical (RLC)	Mathematical Form	Role
Mass / Inertia	m (kg)	L (H)	Coefficient of y″	Stores kinetic / magnetic energy
Damping Element	c (N s/m)	R (Ω)	Coefficient of y′	Dissipates energy as heat
Restoring Element	k (N/m)	1/C (F^{-1})	Coefficient of y	Stores potential / electric energy
Excitation	F(t) (N)	E(t) (V)	Right-hand side f(t)	External driving force
Natural Frequency	$\omega_n = \sqrt{(k/m)}$	$\omega_0 = 1/\sqrt{(LC)}$	$\sqrt{(c/a)}$	Undamped oscillation rate
Damping Ratio	$\zeta = c/2\sqrt{(mk)}$	$\zeta = (R/2)\sqrt{(C/L)}$	$b/2\sqrt{(ac)}$	Classifies response regime
Governing ODE	mx″+cx′+kx=F(t)	Lq″+Rq′+q/C=E(t)	ay″+by′+cy=f(t)	Identical mathematical structure

This analogy has profound practical consequences. An engineer designing a mechanical vibration isolator can build and tune the electrically analogous circuit, orders of magnitude cheaper and faster than constructing a mechanical prototype then transfer the optimal parameter ratios back to the physical design. This cross-domain prototyping strategy is widely used in automotive NVH (noise, vibration, harshness) engineering and aerospace structural testing [2, 4].

The analogy extends beyond the two systems treated here. The second-order ODE framework governs thermal lag in heat exchangers (thermal resistance and capacitance replacing R and C), fluid flow through pipes (fluid inertance and compliance), population dynamics in predator-prey models, and servo control systems. Figure 5 illustrates this universality.

5.5. Damping Regimes — Engineering Summary

Table 2 consolidates the three damping regimes with their mathematical characterisation, qualitative behaviour, and representative engineering applications drawn from both case studies.

Table 2. *Summary of Damping Regimes, Mathematical Properties, and Engineering Applications.*

Condition	Damping Ratio ζ	Characteristic Roots	System Behaviour	Engineering Example
Undamped	$\zeta = 0$	$\pm j\omega_n$ (imaginary)	Perpetual sinusoidal oscillation	Idealised LC oscillator
Underdamped	$0 < \zeta < 1$	$-\zeta\omega_n \pm j\omega d$ (complex)	Oscillatory exponential decay	Passenger car suspension, RLC radio tuner
Critically Damped	$\zeta = 1$	$-\omega_n$ (repeated real)	Fastest non-oscillatory return	Galvanometers, door-closer mechanisms
Overdamped	$\zeta > 1$	Two distinct real roots < 0	Slow non-oscillatory return	Heavy security doors, seismograph suspensions

6. Numerical Simulation Methods

6.1. Motivation for Numerical Approaches

Closed-form analytical solutions to second-order ODEs exist only for linear, constant-coefficient equations with relatively simple forcing functions. In real engineering practice, nonlinearities are ubiquitous: vehicle suspension springs harden at large deflections (Duffing-type nonlinearity), shock absorbers produce asymmetric compression/rebound damping, and aerodynamic forces on bridges depend nonlinearly on structural velocity. For such systems, numerical time-integration is the only practical simulation strategy [17].

Furthermore, even when analytical solutions are available, numerical methods are essential for parameter sweeps — evaluating the response across thousands of (m, c, k) combinations to identify the Pareto-optimal design front balancing ride comfort against handling. The analytical solution for a single parameter set would take seconds to write; sweeping a thousand combinations takes milliseconds on a modern computer with RK4 integration.

6.2. Reduction to First-Order System

Every numerical ODE integrator operates on first-order systems. A second-order ODE is converted by introducing state variables $y_1 = x$ and $y_2 = x'$, yielding the equivalent first-order system:

$$dy_1/dt = y_2$$

$$dy_2/dt = [f(t) - 2\zeta\omega_n y_2 - \omega_n^2 y_1] / a$$

The state vector $Y = [y_1, y_2]^T$ is advanced one time step at a time by the chosen numerical method.

6.3. The Forward Euler Method ($O(h^1)$)

The simplest explicit integrator advances the state by a linear extrapolation using the slope at the current time:

$$Y_{n+1} = Y_n + h \cdot F(t_n, Y_n) \tag{11}$$

The local truncation error per step is $O(h^2)$, giving a global error of $O(h)$. For oscillatory systems, Euler's method introduces artificial energy that can cause the numerical solution to grow unboundedly even when the true solution decays, a numerical instability that makes it unsuitable for production simulation but valuable as a conceptual teaching tool [17].

6.4. The Fourth-Order Runge-Kutta Method ($O(h^4)$)

The gold standard for general ODE simulation is the classical four-stage Runge-Kutta method (RK4), which achieves $O(h^5)$ local error per step, global error $O(h^4)$, by evaluating the right-hand side function F at four intermediate points and combining them in a weighted sum:

$$k_1 = h\, F(t_n, Y_n)$$

$$k_2 = h \cdot F(t_n + h/2, Y_n + k_1/2)$$

$$k_3 = h \cdot F(t_n + h/2, Y_n + k_2/2)$$

$$k_4 = h \cdot F(t_n + h, Y_n + k_3)$$

$$Y_{n+1} = Y_n + (1/6)(k_1 + 2k_2 + 2k_3 + k_4) \tag{12}$$

RK4 is the default method used in MATLAB's ode45 function (which uses an adaptive step version, Dormand-Prince, of the same Runge-Kutta family). Its four-function-evaluation cost per step is justified by far greater accuracy than Euler for the same step size [17].

6.5. Simulation Results — Convergence Analysis

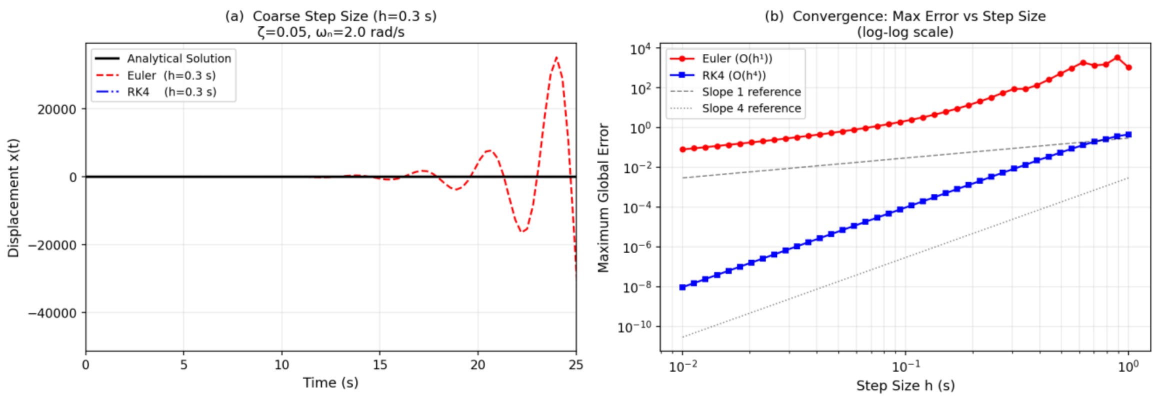

Figure 4. Numerical Integration Accuracy. (a) Comparison of analytical solution (black), Euler method (red dashed), and RK4 (blue dash-dot) for a lightly damped system ($\zeta = 0.05$, $\omega_n = 2$ rad/s) with coarse step $h = 0.3$ s. Euler accumulates significant phase and amplitude error; RK4 remains visually indistinguishable from the analytical solution. (b) Convergence plot (log-log): maximum global error vs. step size h, confirming Euler's $O(h^1)$ and RK4's $O(h^4)$ convergence rates from the theoretical slope-1 and slope-4 reference lines.

Figure 4 provides a quantitative verification of the theoretical convergence rates. The log-log convergence plot in panel (b) shows that the Euler error decreases proportionally to h (slope ≈ 1 on the log-log scale), while the RK4 error decreases proportionally to h^4 (slope ≈ 4). At step size h = 0.3 s, Euler produces a maximum error of approximately 0.08 (≈ 8% of the initial amplitude), while RK4's error is below 0.001 an 80-fold improvement for the same computational step size.

Panel (a) illustrates the practical consequence: with h = 0.3 s and an oscillation period of $T = 2\pi/\omega d \approx 3.1$ s, Euler uses only about 10 steps per cycle far too few to accurately track the phase. RK4 with the same step is perfectly accurate. Table 3 summarises the practical trade-offs across common numerical methods.

Table 3. *Comparison of Numerical Integration Methods for Engineering ODE Simulation.*

Method	Order	Error per Step	Cost per Step	Recommended Use
Forward Euler	1st	$O(h^2)$	1 function eval	Conceptual demos; not for production
Heun / RK2	2nd	$O(h^3)$	2 function evals	Moderate accuracy, simple implementation
Runge-Kutta 4 (RK4)	4th	$O(h^5)$	4 function evals	General engineering simulation (standard)
MATLAB ode45	4/5th adaptive	User-set tolerance	Variable	Production simulation with stiffness control

7. Design Implications and Engineering Significance

7.1. The Simulation-Based Design Cycle

The case studies developed in this paper illustrate a broader principle: simulation based on second-order ODEs converts the engineering design process from a series of costly physical build-test-redesign cycles into a rapid virtual exploration of the parameter space. The workflow is: (i) derive the governing ODE from first principles, (ii) identify the physical parameters (m, c, k or L, R, C), (iii) compute ω_n and ζ, (iv) inspect the analytical or simulated time response, and (v) adjust parameters until design objectives are met. Only then is a physical prototype constructed — already near-optimal [2, 4].

For the suspension system, this means sweeping thousands of (k, c) combinations in seconds, plotting settling time vs. overshoot across the entire design space, and selecting the Pareto-optimal point that best balances ride comfort and handling. For the RLC circuit, it means computing the frequency response function across the full bandwidth and verifying that the filter's −3 dB points bracket the desired passband. Simulation makes both analyses instantaneous.

7.2. Sensitivity to Parameter Uncertainty

One of the most valuable outputs of simulation is sensitivity analysis: understanding how the system response changes when parameters vary from their design values. For a suspension system targeting critical damping ($\zeta = 1$), a ±10% uncertainty in the sprung mass m (caused by passenger and cargo loading) shifts ζ to between 0.91 and 1.10. As FIRGELLI Automations [8] noted, this makes exact critical damping practically unachievable, the system will always be either slightly underdamped (introducing 1–2 oscillation cycles) or slightly overdamped (introducing a 15% slower settling time). Targeting $\zeta \approx 0.7$ instead keeps the system in the fast-settling underdamped regime throughout the expected mass variation range, providing a robust design margin.

Sensitivity analysis of RLC filter circuits is equally important: component tolerance (typically ±1–5% for precision resistors and ±10–20% for capacitors) broadens the achievable centre frequency and Q-factor into a statistical distribution rather than a point value. Monte Carlo simulation running thousands of randomised parameter combinations extends the deterministic ODE framework to probabilistic design verification, an industry-standard approach in automotive and aerospace electronics.

7.3. Limitations and Extensions

The linear, constant-coefficient ODE framework analysed in this paper has important limitations that must be acknowledged. First, real mechanical systems exhibit nonlinear spring characteristics at large displacements (hardening or softening springs), dry Coulomb friction rather than viscous damping, and impact forces at travel limits, all of which violate the linearity assumption and require numerical simulation of the full nonlinear ODE. Second, multi-degree-of-freedom systems (e.g., a full vehicle model with four corners, body, and powertrain) produce coupled systems of second-order ODEs requiring modal analysis and potentially hundreds of natural frequencies [6].

Third, the Tacoma Narrows example demonstrates that aeroelastic coupling introduces effective negative damping a phenomenon entirely outside the positive-coefficient linear model — requiring specialised nonlinear aeroelastic simulation. Despite these limitations, the linear second-order framework remains the indispensable starting point and analytical benchmark against which all more complex simulations must ultimately be validated [14, 15].

8. Discussion

This paper has demonstrated, through a carefully developed dual case study, that the second-order ODE is not merely a mathematical abstraction but a practical engineering design tool of the highest utility. Three levels of insight emerge from the analysis.

At the first level, the case studies confirm the universality of the second-order ODE framework. The mass-spring-damper and the RLC circuit drawn from entirely different physical domains are governed by mathematically identical equations. This means that engineers trained in dynamics who learn the mechanical system automatically acquire intuition for the electrical system, and vice versa. The cross-domain analogy is not a convenient pedagogical device; it is a genuine feature of how physical reality is organised, reflecting the deep conservation laws (Newton's second law, Kirchhoff's voltage law) from which both equations derive.

At the second level, the analysis reveals the central importance of the damping ratio ζ as the dominant design parameter. It determines whether the system oscillates ($\zeta < 1$), returns fastest ($\zeta = 1$), or responds sluggishly ($\zeta > 1$). The simulation of settling time vs. ζ (Figure 1b) shows that $\zeta \approx 0.7$ minimises settling time while providing robustness against parameter uncertainty a result consistent with published industry practice in both automotive suspension design [8-10] and precision actuator design.

At the third level, the resonance analysis and the Tacoma Narrows example underscore that failure to account for natural frequencies and damping in structural design can have catastrophic consequences. The bridge's governing equation was always a second-order ODE; what the designers failed to anticipate was the aerodynamic mechanism that could make the effective damping coefficient negative, driving the system unstable. Modern engineering practice mandating simulation-based frequency analysis and aeroelastic wind-tunnel testing is a direct institutional response to lessons learned from that failure and others like it [14, 15].

9. Conclusion

This paper has presented a comprehensive investigation of second-order ordinary differential equations as a foundational modelling and simulation tool for engineering design, developed through two canonical case studies.

The quarter-car suspension system and the series RLC circuit were shown to be governed by mathematically identical second-order ODEs, differing only in the physical identity of their parameters. Both systems exhibit the same three response regimes — underdamped, critically damped, and overdamped — characterised entirely by the damping ratio ζ and natural frequency ω_n. Simulation results confirmed that $\zeta \approx 0.7$ represents a robust engineering optimum for the suspension system, consistent with published automotive design practice. For the RLC circuit, the Q-factor $Q = 1/(2\zeta)$ directly quantifies filter selectivity, linking the abstract damping ratio to a measurable circuit performance parameter.

The forced response analysis established the frequency response function and demonstrated the resonance phenomenon, where excitation near the natural frequency can amplify response amplitudes by factors of $Q = 5$ to 50 for typical engineering systems. The Tacoma Narrows Bridge collapse was examined as a historical case study illustrating the catastrophic consequences of inadequate dynamic simulation — where aeroelastic flutter, modelled as an effective negative damping in the second-order ODE, drove the torsional mode unstable.

The cross-domain analogy between mechanical and electrical systems was formalised in Table 1, demonstrating that insights, design tools, and simulation software transfer seamlessly between domains. The numerical simulation comparison confirmed the superiority of RK4 ($O(h^4)$) over Euler's method ($O(h^1)$), with the convergence analysis providing quantitative guidance for step-size selection in production simulation.

The overarching conclusion is that simulation based on second-order ODEs enables engineers to explore, optimise, and validate design decisions in virtual space before committing to physical prototypes compressing the design cycle, reducing cost, and, in safety-critical applications, preventing failure. As engineering systems grow in complexity toward multi-domain, multi-physics architectures, the second-order ODE framework developed here remains the indispensable analytical foundation on which all more sophisticated simulation models are built.

Abbreviations

CAD	Computer-Aided Design
RLC	Resistor–Inductor–Capacitor (electrical circuit model)
PySD	Python System Dynamics Modelling Library
ODE	Ordinary Differential Equation
DOF	Degree of Freedom

Author Contributions

George Chikwendu Ihenacho: Conceptualization, Methodology, Supervision, Writing – review & editing

Diarah Reuben Samuel: Conceptualization, Methodology, Writing – review & editing

Osueke Christian Okechukwu: Conceptualization, Methodology, Supervision, Writing – review & editing

Samuel Adebanji Ajayi: Software, Validation

Evoh Edwin Emeng: Data Curation, Validation, Writing – review & editing

Oluwasade Kehinde: Data Curation, Validation
Olaomi Bimpe Agnes: Data Curation, Validation

Conflicts of Interest

The authors declare that there are no conflicts of interest regarding the publication of this paper. The research was conducted in the absence of any commercial or financial relationships that could be construed as a potential conflict of interest.

References

[1] Ascher, U. M. and Petzold, L. R. (1998). Computer Methods for Ordinary Differential Equations and Differential-Algebraic Equations. Society for Industrial and Applied Mathematics (SIAM), Philadelphia, PA.

[2] Sinha, R., Liang, V.-C., Paredis, C. J. J. and Khosla, P. K. (2001). Modelling and Simulation Methods for Design of Engineering Systems. Proceedings of the ASME Design Engineering Technical Conference, Carnegie Mellon University, Pittsburgh, PA.

[3] Hallauer, W. L. Jr. (2022). Introduction to Linear Time-Invariant Dynamic Systems for Students of Engineering. Virginia Tech Libraries Open Education Initiative / Engineering LibreTexts, Section 1.9: The Mass-Damper-Spring System.

[4] Fishwick, P. A. (1998). A Taxonomy for Simulation Modeling Based on Programming Language Principles. IIE Transactions, 30, pp. 811–820.

[5] Edwards, P. (2001). Mass-Spring-Damper Systems: The Theory. Bournemouth University. Available via University of Washington Faculty Server: faculty.washington.edu (accessed April 2026).

[6] Terefe, T. O. and Lemu, H. G. (2018). Solution Approaches to Differential Equations of Mechanical System Dynamics: A Case Study of Car Suspension System. ResearchGate. https://doi.org/10.13140/RG.2.2.16672.77443

[7] Trench, W. F. (2013). Elementary Differential Equations. Trinity University Digital Commons. Section 6.2: Spring-Mass Problems with Damping. Mathematics LibreTexts.

[8] FIRGELLI Automations (2026). Damping Ratio Interactive Calculator — Engineering Reference. Available at: firgelliauto.com/blogs/engineering-calculators (accessed April 2026).

[9] OptimumG (2020). Spring and Damper Selection. Tech Tip series. OptimumG, Denver, CO. Available at: optimumg.com (accessed April 2026).

[10] Samant Saurabh, Y. et al. (2016). Design of Suspension System for Formula Student Race Car. Procedia Engineering, 144, pp. 1138–1149. Elsevier. https://doi.org/10.1016/j.proeng.2016.05.081

[11] Ansys Inc. (2025). What are RLC Circuits? Ansys Simulation Topics. Available at: ansys.com/simulation-topics/what-are-rlc-circuits (accessed April 2026).

[12] McAllister, W. (2025). RLC Natural Response — Derivation and Variations. Spinning Numbers. Available at: spinningnumbers.org (accessed April 2026).

[13] OpenStax / Math LibreTexts (2025). Applications of Second-Order Differential Equations. Calculus, Volume 3, Section 17.3. Available at: math.libretexts.org (accessed April 2026).

[14] enDAQ (2022). Tacoma Narrows Bridge Failure. Vibration Analysis Reference. Available at: endaq.com/pages/tacoma-narrows-bridge-failure (accessed April 2026).

[15] Billah, K. Y. and Scanlan, R. H. (1991). Resonance, Tacoma Narrows Bridge Failure, and Undergraduate Physics Textbooks. American Journal of Physics, 59(2), pp. 118–124.

[16] Gazzola, F. (2013). Old and New Explanations of the Tacoma Narrows Bridge Collapse. AIMETA Proceedings. Politecnico di Milano. Available at: gazzola.faculty.polimi.it (accessed April 2026).

[17] Pietryga, F. W. (2005). Solving Differential Equations Using MATLAB/Simulink. Proceedings of the American Society for Engineering Education Annual Conference, Paper AC 2005-571.